# Data Acquisition System And Methodology for High Angle Of Attack Parameter Estimation

**By M. Sri-Jayantha and Robert F. Stengel**

**Princeton University**
**Princeton, New Jersey**

## ABSTRACT

A digital data acquisition system that has been flight tested in a Schweizer 2-32 sailplane, and the algorithms designed for high angle of attack parameter identification, are described in this paper. The system is portable and self-contained. Inertial sensors are mounted in a strapdown unit. Two Kiel-probes are used for airspeed measurement. "Off-the-shelf" microelectronics components are configured to operate as a multiprocessing system. The on-board computing power is used to monitor the sensor and support system and to improve flight test effectiveness. The Estimation-Before-Modeling technique has been selected for parameter identification. A time history of a flight test maneuver that will be used in the estimation of the aerodynamic parameters is also presented.


Knowledge of aerodynamic parameters is essential for simulation, control system design, specification, and stability analysis of modern aircraft. Aerodynamic parameter identification at high angles of attack and sideslip is particularly difficult because aerodynamic forces and moments are nonlinear functions of motion and control variables. This paper focuses on solving the high angle-of-attack-dynamics instrumentation, data acquisition, flight testing, and parameter identification problems. Aerodynamic parameters are typically determined from wind-tunnel tests. The differences that exist between the wind-tunnel test and flight conditions offer sufficient motivation for determining the parameters from flight data.[1] The elements involved in an aircraft parameter estimation (or identification) problem are illustrated in **Figure 1**.

At high angles of attack and sideslip, as in stalls and spins, the following aspects of the aerodynamic parameter identification problem should be taken into consideration:

- selection and design of instrumentation for large amplitude motion variables,
- design of a cost-effective data acquisition system,
- effect of nonlinear aircraft dynamics arising from large perturbation in states,
- modeling of significant longitudinal and lateral coupling though inertial, aerodynamic and kinematic components of motion,
- estimation of nonlinear aerodynamics with possible discontinuities (e.g., hysterises in wing rock),
- elimination of singularity associated with Euler angles at large pitch attitude,
- selection and implementation of parameters identification algorithms, and
- design of flight test maneuvers.

The inherent nonlinearity in the equation of motion, kinematics, and aerodynamics due to high angle of dynamics is accommodated by employing *Estimation Before Modeling* (EBM) as the identification technique.[2] This method has been used previously at the Flight Research Laboratory to identify the aerodynamic parameters of the Avionics Research Aircraft (ARA), a highly modified Navion.[3] The conventional Euler angles are replaced by *quaternions* in the attitude kinematic model.[4] The strapdown scheme eliminates the need for attitude gyros, and the singularity-free quaternion has improved accuracy over the conventional Euler angle formulation. The EBM technique uses an Extended Kalman Filter (EKF) and a modified Bryson-Frazier Smoother (MBFS) to compute the aerodynamic forces and moments in the time domain. The statistically optimal estimates are subsequently used to extract the aerodynamic models using a linear regression method. The structure of the parameter identification algorithms and an example of a Schweizer 2-32 sailplane maneuver time history are presented.

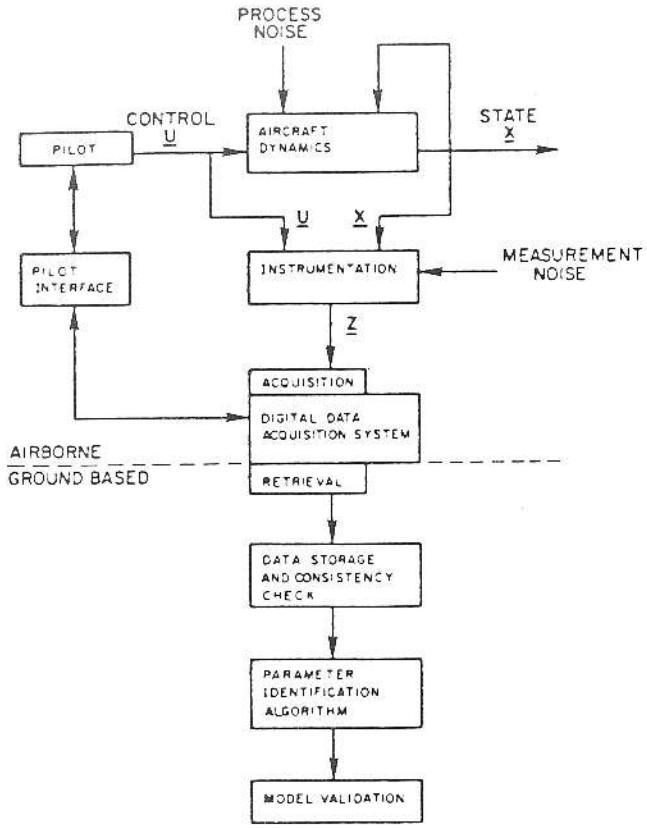


**Figure 1: Elements of Parameter Identification**

The instrumentation package contains two air data units (ADU), an inertial measurement unit (IMU), and control surface displacement sensors. The data acquisition system is microprocessor-based, and is programmed to operate in several modes. In the flight test mode, it collects data from 21 sensors at a rate of 20 samples per sec. The computer system also is used to monitor the sensors, and to improve the flight test effectiveness. Design of the data acquisition system is described in detail.

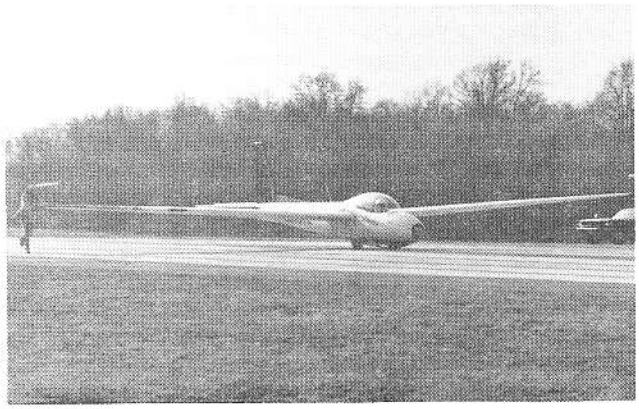

**Figure 2: Instrumented Schweizer 2-32 Sailplane**

## FLIGHT TEST VEHICLE

A Schweizer 2-32 sailplane is used as the test vehicle (**Figure 2**). The two-place sailplane was chosen for several reasons: the absence of powerplant effects simplifies parameter identification, the aircraft is relatively safe to stall and spin, and the aerodynamic results are of interest.

## SELECTION OF AN IDENTIFICATION METHOD

Techniques for parameter estimation have been used in several disciplines, such as econometrics, biology, and engineering; consequently, the literature on this subject is abundant, and sometimes confusing. Aircraft parameter identification methodology has evolved from the use of static maneuvers through frequency testing to transient dynamic flight testing.[5] With the advent of high-speed digital computers, it has become much more sophisticated and specialized. The Maximum Likelihood Method is the most prevalent technique in aeronautics.[6] Other parameter identification methods that are attractive for digital computer implementation are the Extended Kalman Filter and Estimation-Before-Modeling approaches.[2] Note that an EKF can be used as an independent technique for parameter identification; nevertheless, it also is used in both Maximum Likelihood and Estimation-Before-Modeling methods for intermediate computations.

When the Maximum Likelihood or EKF method is used, the model structure of the unknown aerodynamic forces and moments *must be* specified prior to the parameter identification algorithm design. If a different model structure is deemed necessary to accommodate specific maneuvers or aerodynamic assumptions, the algorithms must be reformulated. Unlike the Maximum Likelihood and EKF methods (where the state and parameter estimation are simultaneously performed), Estimation-Before-Modeling is a two-step procedure. The state estimation and the aerodynamic model determination are carried out independently. The aerodynamic forces and movements are estimated, using filtering and smoothing, as time functions with only inertial and gravity effects modeled in the dynamic equations. Consequently, model structures for the aerodynamics forces and moments are not selected prior to estimation. In the second step, the aerodynamic model structure is determined using multiple regression techniques; hence, simple models can be employed, by dividing the data base into "subspaces." The nonlinearities arising from high angles of attack can be modeled with a few parameters for each subspace. Therefor, Estimation-Before-Modeling has been chosen as the identification method.

The basic idea behind the two-step identification procedure has been in existence for some time.[7-10] The method used to estimate the forces and moments has been modified so that state-variable filtering and smoothing has been applied in the EBM procedure.[2] The principle of this procedure is illustrated in **Figure 3**. The estimation of the aerodynamic forces and moments is accomplished in a general framework, where the dynamics and measurements are allowed to contain stochastic components. The unknown time histories of the forces and moments are modeled as higher-order Gauss-Markov processes. It is important to distinguish between the first-order Gauss-Markov description of the basic airframe dynamics and the higher Gauss-Markov modeling of the unknown aerodynamic forces and moments.

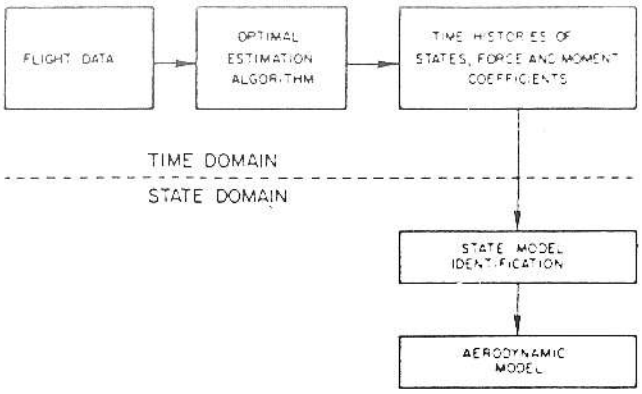


**Figure 3: The Estimation-Before-Modeling Methodology**

## BRIEF MATHEMATICAL DESCRIPTION

The aircraft dynamics are described by a vector nonlinear differential equation:

$$\dot{\underline{x}}(t) = \underline{f}[\underline{x}(t), \underline{B}(t)] + \underline{w}(t) \qquad (1)$$

The state vector, $\underline{x}$, has 11 components; they are three angular rates, three linear velocities, four quaternion components, and altitude. The position of the aircraft in the horizontal plane is not relevant for aerodynamic parameter identification, although it must be known to account properly for the effects of gravity. The vector $\underline{B}(t)$ represents the six aerodynamic forces and moments about the body axes of the aircraft. Unmeasurable disturbances and model deficiencies are represented by the "process noise" vector, $\underline{w}(t)$.

The measurements are sampled when a digital data acquisition is used. The sensor information is related to the system state and force vectors by the following algebraic equation:

$$\underline{z}(t_k) = \underline{h}[\underline{x}(t_k), \underline{B}(t_k)] + \underline{v}(t_k) \quad (2)$$

The vector dimension of this equation is determined by the number of sensors employed and the parameter identification method used. Typically, the dimension is between 10 and 30. The measurement inaccuracies are represented by the "measurement noise" vector, $\underline{v}(t_k)$.

## INSTRUMENT AND DATA ACQUISITION

The special purpose data acquisition system is referred to as Micro-MAP (Microprocessor-based system for the Measurement of Aerodynamic Parameters). The fundamental purpose of Micro-MAP is to acquire the time sequence of the measurement vector $z(t_k)$ of eq. (2) corresponding to a flight test maneuver. It is accomplished by sampling, digitizing, and recording operations. Many of the Micro-MAP components were tested in the previous ARA parameter identifications.[3]

In addition to these basic operations, the Micro-MAP is designed with sensor and support system "health" monitoring and testing, pilot cueing for effective flight tests, and in-flight data quality evaluation using the Fisher Information Matrix.[11] The Micro-MAP is designed so that it can be installed in another aircraft with ease. This portability is achieved by keeping the hardware modular and by the software on-board bootstrap operation described below.

**Menu Driven Data Acquisition System**—Various modes of the Micro-MAP are shown in **Figure 4**. Each mode can be invoked either in flight or on the ground, as required. Data acquisition and sensor monitoring are the most critical design consideration for the Micro-MAP. Beyond these, the system should be easy to learn and easy to use. Multiple menus are arranged and presented to the test pilot in a tree-like structure. The test pilot first selects any one of the items on the top-level menu. As a response to this, the second-level menu is displayed. This process of directing the computer is called Menu Traversing. As an example, the first-level menu is presented:

Micro-MAP Control:
F,L,M,S,T,X=*?
F=Flight Test Mode
L=Load Point Tape (Initialize)
M=Menu Display
S=Send Data To Ground Computer
T=Subsystem Testing Mode
X=Exit to System Monitor

For example, if the pilot enters "F", the system will request the flight number, data track number, etc. If he enters "T", it will display the possible tests he could perform using the Micro-MAP.

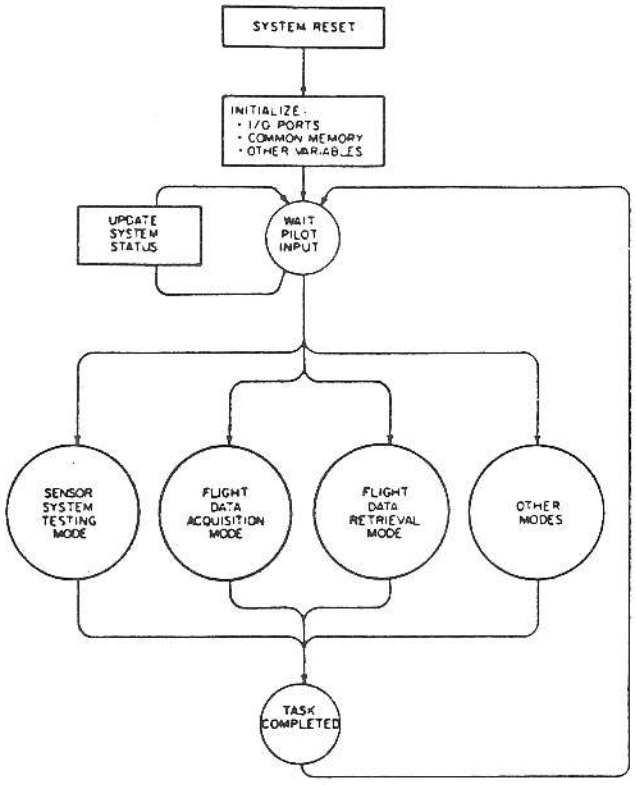


Figure 4: Modes of the Micro-MAP

**Micro-MAP Hardware and Architecture**—the Micro-MAP consists of several components, as shown in **Figure 5**. The computer system architecture is shown in **Figure 6**. The CPU's #0 and #1, 4K RAM, ADC and DAC, and Bessel filter all are Multibus®-compatible boards. The five Multibus boards are housed in a radio-frequency-shielded aluminum box. The system status messages are displayed through eight LEDs located in the cockpit. The CDU provides the input and/or output (I/O) interface between the pilot and the Micro-MAP. An electrostatic printer generates a printed copy of all the messages displayed on the CDU.

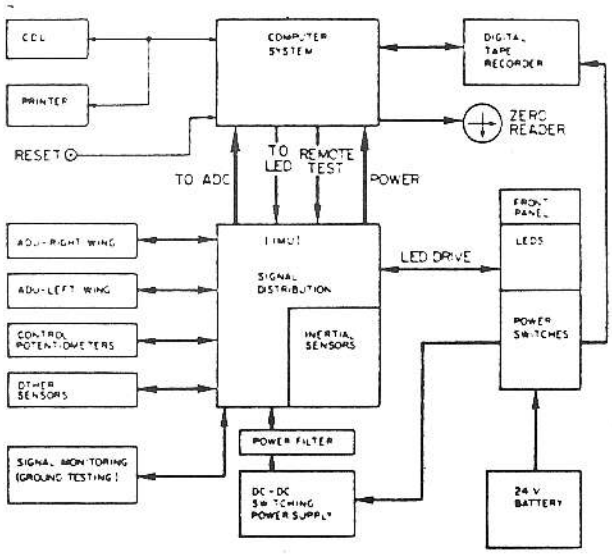


Figure 5: Micro-Map Hardware

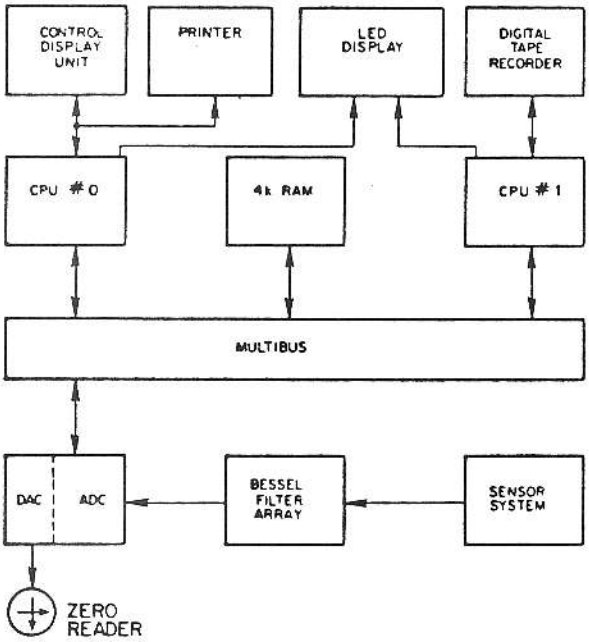


Figure 6: Micro-MAP Architecture, Two Processor Design

The digital cartridge tape recorder is a 4-track, 1600-bits-per-inch unit with a transfer rate of 6K bytes/second. The tape control task is dedicated to CPU #1, which executes custom-designed software. The main processor determines the sequence of operations necessary, then sets the appropriate "control code" in the shared memory.

The "zero ready" has both horizontal and vertical indicators that are driven by independent voltage inputs. The zero reader displays the sensor outputs with CPU #0 in the loop; during flight testing, it displays the average angle of attack and sideslip measured by the wing tip ADUs.

Two 12v "gelcell" batteries provide the power source. A DC-DC switching power supply provided the +28 and +/-12 volt outputs. Another regulator located within the inertial

measurement unit is driven by a regulated 28v line; it powers the control surface and ADU potentiometers with +/-15v. The inherent ripple of the DC-DC power supply is reduced by a C-L-C power filter. Additional capacitive filtering is used to prevent transient effects at the input and output of the tape power supply.

## BOOTSTRAP OPERATION

The software of the Micro-MAP is coded in Assembly and Pascal languages (**Table 1**). Pascal is used for the main control software, where floating point operations and extensive input/output operations are carried out. Time and storage-critical tape control tasks are programmed in Assembly language.

| Language | CPU | Memory | Routine |
|---|---|---|---|
| Pascal | 0 | RAM 30K | Main Control |
| Assembly | 0 | PROM 2K | Monitor |
| Assembly | 0 | PROM 2K | Bootstrap |
| Assembly | 1 | PROM 2K | Tape Control |

**Table 1: Software Used in the Micro-MAP**

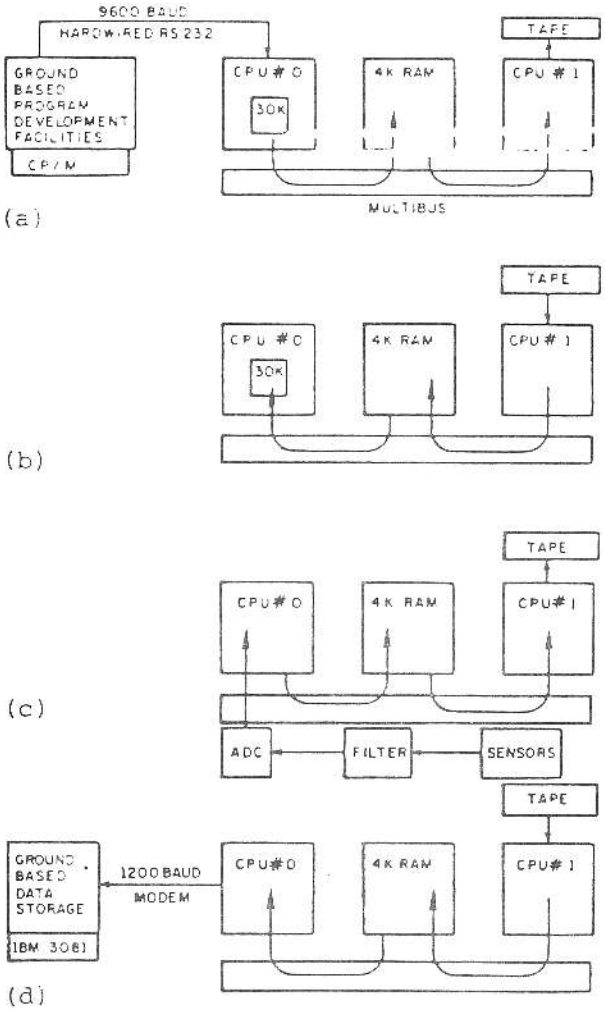


**Figure 7: Data Paths; (a) Program storage, (b) Bootstrap, (c) Data acquisition, and (d) Data retrieval.**

It is highly inflexible and inefficient to store the main control program (30k bytes) in a PROM. The control program can either be loaded into the Micro-MAP RAM from a ground computer prior to the flight test or by using an on-board bootstrap feature. The bootstrap method used in the Micro-MAP and the paths taken by the data during various modes are shown in **Figure 7**. This enables the limited on-board battery power to be conserved until the sailplane is ready for flight testing, i.e., after the towing phase of the flight has been completed. The memory space allocation is defined in **Figure 8**.

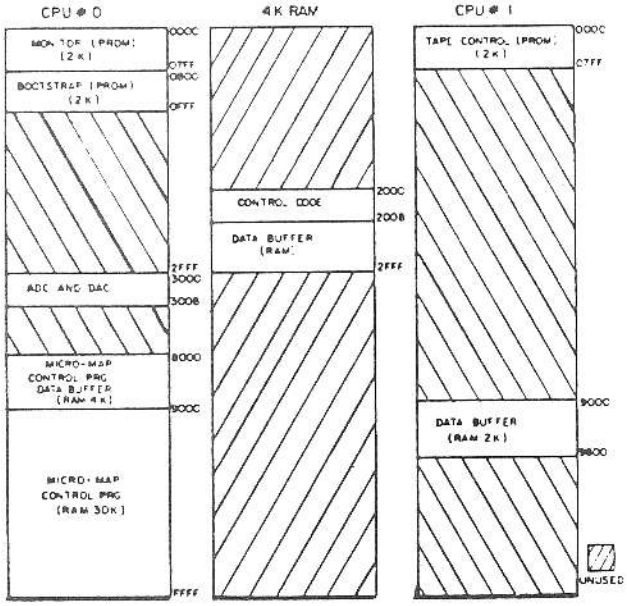


**Figure 8: Memory Space Allocation**

The system Monitor simplifies the trouble-shooting task. As an example, when the shared memory was introduced to exchange information between CPU #0 and CPU #1, the memory dump command of the Monitor proved to be very useful. With all the software/hardware deficiencies corrected and refined, the Monitor can be removed from the software library.

**Timing Diagram of Micro-MAP**—Among the modes of operation, data acquisition is the most time-critical. There are two time constraints associated with this mode. The rate at which data is generated must be less than the rate at which it can be recorded. This is not a problem in the Micro-MAP, where the maximum possible rate of recording is 6K bytes/sec and the rate of generation is only 1K bytes/sec (at 20 samples per second.) The data accumulated over a fixed period of time must be transferred to the shared memory within the idle time between two samples. In the Micro-MAP, the idle time is 28 msec, and the transfer time of 1K byte of data accumulated over 1 sec duration is 7 msec.

Since a recorded block of data contains 2K bytes, the data transfer to CPU #1 from CPU #0 is carried out in two 1K-blocks per 2K-block of data. **Figure 9** illustrates the timing sequence during the flight data acquisition mode. The beginning of each block is prepared with flight number, maneuver number, etc., so that the data block can be easily stored and retrieved without extensive documentation. One track of a cartridge can contain 600 sec of flight data.

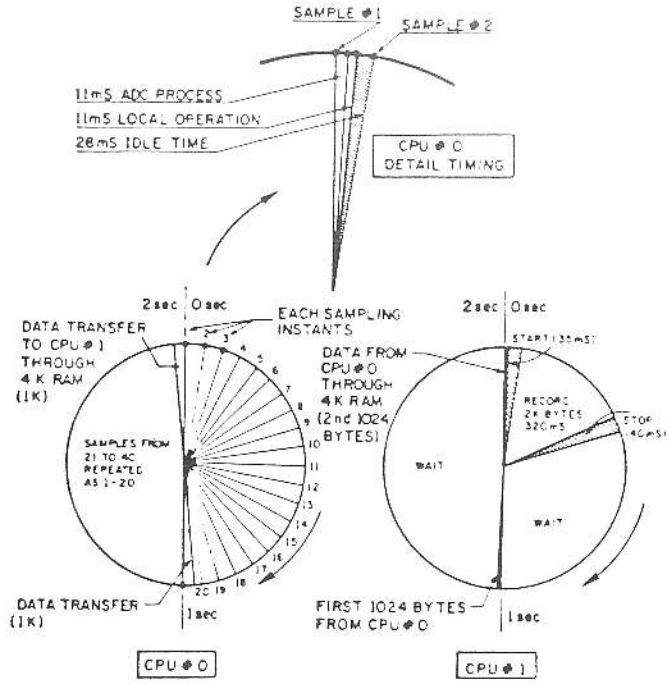


Figure 9: Timing Diagram of Micro-MAP

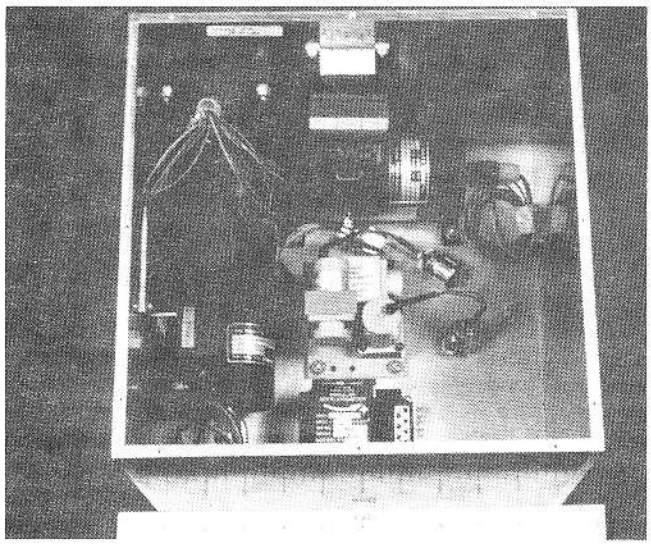

Figure 10: Micro-MAP Inertial Measurement Unit

**Aircraft Instrumentation**—The sensors required to provide useful information about the aircraft dynamics are classified into three groups: inertial, air data, and control displacement. The inertial sensors (3 linear accelerometers, 3 angular rate gyros, and 3 angular accelerometers) are rigidly and orthogonally mounted in the IMU, shown in **Figure 10**. It weights 20 lb., measures 10″×10″×8″, and is located near the aircraft's center of gravity. The position effects on the linear acceleration measurements are modeled in the nonlinear measurement (eq. (2)). The IMU also serves as the junction box through which the Micro-MAP sensor system signal and power lines are routed. The hardware design is modularized by this approach.

The air data sensors provide angle-of-attack, sideslip angle, dynamic pressure, and static pressure measurements. The four sensors are integrated into one unit called an ADU. There are two ADUs, one on each wing tip, as shown in

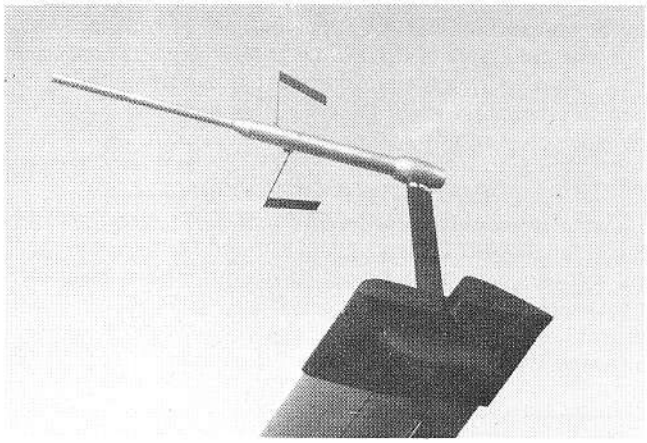

Figure 11: Wing-Tip-Mounted Air Data Unit

**Figure 11**. Flow interference effects are reduced by locating the sensors upstream of and above the leading edge at a distance more than one-and-on-half times local chord.[12] To minimize transport lag, the pressure transducers are located at the wing tip in proximity to the sensing ports. Shrouding the pitot tube reduces its sensitivity to flow incidence angle. Wind-tunnel tests performed on this unit, which is called a Kiel probe, indicate that the useful range of total pressure measurement is about 62 degrees of low angle. However, the static pressure measurement continues to be sensitive to flow incidence angle. Note that the flow incidence angle is a transcendental function of the angle of attack and sideslip angle. The wind-tunnel results are shown in **Figure 12**, and the test details are documented in Reference 13. A 99% curve fit on the wind tunnel data is obtained using a quadratic model for the static and dynamic pressure:

$$(p_s)_{corrected} = p_s\ (0.98 + 0.46\,\lambda) \quad (3)$$

$$(p_d)_{corrected} = p_d\ (1.028 - 0.48\,\lambda) \quad (4)$$

The control surface displacement sensors are special purpose potentiometers attached to the mechanical linkages driving the four control surfaces. The proximity of the potentiometers to the control surfaces reduces the effect of control cable dynamics.

In order to minimize the influence of sensor dynamics, the natural frequency of the sensors should be large. Higher bandwidth provides constant dynamic gain and linear phase lag over the frequency range of interest; however, structural vibrations and turbulence-induced high frequency dynamics are also captured by the sensors. Undesirable high frequency components are excluded from the sampling process by an analog prefiltering operation.

**Presampling Filter and Sampling Rate Selection**—Errors of commission and omission are inherent in a digital sampling process.[14] The two errors can be minimized by the choice of sampling rate and presampling filter. It is difficult to formulate a uniform method for sampling rate selection.[15] For a short period mode with a 1.5 Hz natural frequency or less, a sampling rate of 20 samples per sec is high enough if the noise bandwidth is kept below the Nyquist frequency of 10 Hz. The DC-DC power supply has a narrowband spectrum at 25 KHz, and the sailplane structural modes are presumed to be above 6Hz; hence, a Bessel filter with a cutoff frequency of 6.5 Hz is employed. The Bessel

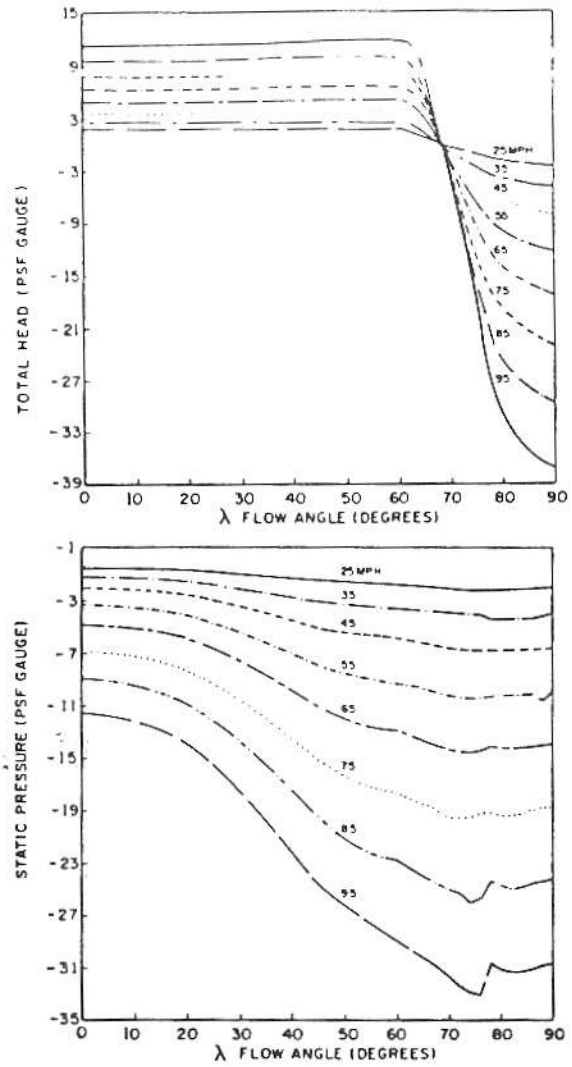


Figure 12: Wind Tunnel Test Results of ADU

filter transfer function defined below has the best phase lag characteristics, in the sense that all the frequency components in the pass band are delayed by an equal amount.

$$H(s) = \frac{1}{[(s/w)^2 + \sqrt{3}(s/w) + 1]} \qquad (5)$$

The filter is implemented with an equivalent time delay of 43 ms. Since identical filters are used on all data channels, the filter lag does not affect the cause-and-effect relationship of the dynamic system described by eq. (1) and (2). Relative delay between different channels due to the sensor dynamics can be harmful, and serious errors in the parameter estimates can result.[16]

**Calibration** Sensor outputs are scaled to a +/-10V range to be compatible with the ADC. The filter board also is designed with bias and gain adjust features for calibration (**Figure 13**). Inertial sensors can be tedious to calibrate, and manufacturer's data should be modified to account for the presence of bias and gain. The calibration of the Micro-MAP was performed at an input supply voltage of 23V to represent an actual field condition. The ADU sensors are tested for leakage and clogged tubing.

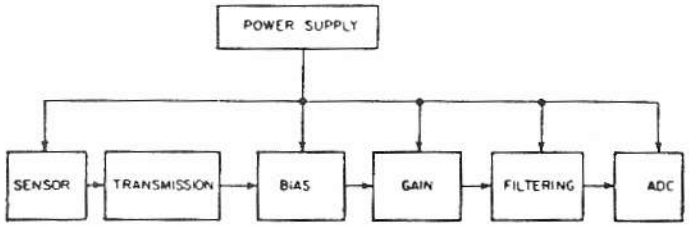


Figure 13: Calibration Components

**Fault Detection and System Health Monitoring** In developing Micro-MAP software, we are faced with the difficult question of how to validate the integrated system in a realistic environment. Flight testing costs may be too high to perform a series of actual flight tests in order to validate the Micro-MAP. Simple statistical parameters, namely, the mean and the standard deviation, are computed to judge sensor performance in the Micro-MAP.

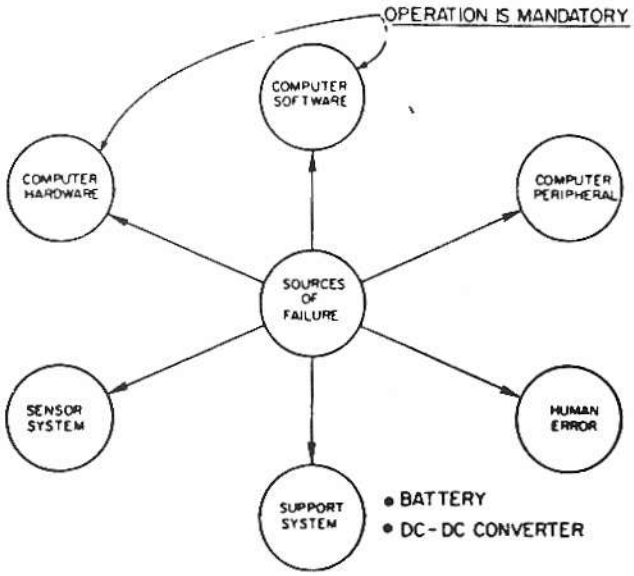


Figure 14: Micro-MAP Subsystems Subject to Failure

A system failure can arise from any of the subsystems illustrated in **Figure 14**. In the design of the Micro-MAP we have assumed that the probability of partial or total failure of the Micro-MAP due to computer failure is minimal. In order to monitor the computer system, two LEDs on the front panel are activated by the computers when they are in the quiescent state. In the data acquisition mode, the LEDs are activated at a different rate, confirming the proper functioning of the computers plus the shared memory. A completion of the bootstrap operation would imply that the data storage device (i.e., the recorder), also is in operation.

The sensor system is monitored by providing the pilot with a set of commands which allow the pilot to make a judgment about the quality of sensor performance. The possible operations are:

- Monitor a single channel continuously. (For example, the pilot may move the rudder pedals and observe the voltage display on CDU or on the zero reader.
- Compute a 25-sample mean of all the sensors and generate a printout in engineering units. This helps to estimate instrument bias for later parameters identification on the ground.

- Compute the noise statistics of all the sensors (standard deviation).
- Use sensor remote test features to perform a test, and compare the results with a known measurement. (The remote test is automated).

Recursive algorithms are used to compute the statistical parameters, with the assumption of stationary noise sequences.

The power supply requirements are monitored continuously by the computer. The battery closed circuit voltage (at a load of 8 Amp) may drop below a predetermined threshold value (19V). If this occurs, one LED allocated for the "power" is switched off. In the implementation, the 28V and +/-15V lines also are monitored. Since the power supply levels are very crucial to the accuracy of sensor measurements, a routine also is provided to compute the noise standard deviation of the four power levels. For a given threshold setting and noise standard deviation, the false alarm and miss alarm probabilities can be computed.

Inadvertent keyboard entry can occur. In critical branches of the software where an error committed may not be corrected, double stroke entries are required.

## PARAMETER IDENTIFICATION METHODOLOGY

The Estimation-Before-Modeling technique will be applied to extract aerodynamic parameters.[2] The structure of the identification algorithms, and a flight test time history are presented in this section.

**Problem Formulation**—the aircraft dynamics represented by eq. (1) along with a model for the aerodynamical forces and moments are described by a set of continuous nonlinear stochastic ordinary differential equations:

$$\begin{bmatrix} \dot{\underline{x}} \\ \dot{\underline{B}} \end{bmatrix} = \begin{bmatrix} \underline{f}[\underline{x}(t), \underline{B}(t)] \\ L\ \underline{B}(t) \end{bmatrix} + \underline{w}(t) \qquad (6)$$

A single force or moment component is described by eq. (7) as a third-order Gauss-Markov process. The first element of the vector $\underline{B}_i$ is one of the six aerodynamic components,

$$\dot{\underline{B}}_i = L_i\ \underline{B}_i + \underline{w}_i\ (t) \qquad (7)$$

where

$$L_i = \begin{bmatrix} 0 & 1 & 0 \\ 0 & 0 & 1 \\ 0 & 0 & 0 \end{bmatrix} \qquad (8)$$

The block matrix L is assembled from the $L_i$ as follows:

$$L = \left[\begin{array}{c|c|c|c|c|c} L_1 & 0 & 0 & 0 & 0 & 0 \\ \hline 0 & L_2 & 0 & 0 & 0 & 0 \\ \hline 0 & 0 & L_3 & 0 & 0 & 0 \\ \hline 0 & 0 & 0 & L_4 & 0 & 0 \\ \hline 0 & 0 & 0 & 0 & L_5 & 0 \\ \hline 0 & 0 & 0 & 0 & 0 & L_6 \end{array}\right] \qquad (9)$$

The best model of B suitable for aircraft parameters identification, and the questions of observability and identifiability, are important theoretical problems that remain to be solved.

**Filtering and Smoothing**—The optimal estimate of the augmented state vector of eq. (6) (denoted by $\underline{x}$ for conciseness in this section) is achieved using an Extended Kalman Filter and a Modified Bryson-Frazier Smoother. The Extended Kalman Filter is implemented as follows:[17]

**Initial Condition**—the $\underline{x}_0$ and $P_0$ are computed using 100 samples of trim data preceding each maneuver. The initial condition may change from one maneuver to another.

**Process and Measurement Noise**—Matrices Q and R are obtained through prior tuning and engineering judgement. Once they are selected, they are not adjusted, unless the flight conditions have changed drastically (e.g., due to turbulence level).

**State and Covariance Extrapolation**—The numerical integration of eq. (10) and (11) from $t_k(+)$ to $t_{k+1}(-)$ is performed using a double-precision (64 bit) fourth-order Runge-Kutta integration scheme,

$$\dot{\underline{x}} = \underline{f}(\underline{x}, t) \qquad (10)$$

$$\dot{P} = FP + PF^T + Q \qquad (11)$$

where

$$F = \left.\frac{\partial \underline{f}}{\partial \underline{x}}\right|_{\underline{x}_k(t)} \qquad (12)$$

Note that the dynamic system is linearized in eq. (12) about the current value of $\underline{x}(t)$. In eq. (10) the function $\underline{f}$ represents the augmented system of eq. (6). The four quaternions are normalized after the extrapolation.

**Kalman Gain Matrix**—

$$K_k = P_k(-) H_k^T(-) [H_k(-) P_k(-) H_k^T + R_k]^{-1} \qquad (13)$$

where

$$H_k = \left.\frac{\partial \underline{h}}{\partial \underline{x}}\right|_{\underline{x}_k(-)} \qquad (14)$$

**State and Covariance Update**—

$$\underline{x}_k(+) = \underline{x}_k(-) + K_k[\underline{z}_k - \underline{h}(\underline{x}_k(-))] \qquad (15)$$

$$P_k(+) = [I - K_k H_k(\underline{x}_k(-))] P_k(-) \qquad (16)$$

Numerical stability problems associated with the covariance update (eq. (16)) are suppressed by employing double-precision arithmetic. Methods such as square-root filtering or $UDU^T$ factorization can also be used with increased computational efficiency.[18-19] The gradient matrices given by eq. (12) and (14) are sparse,

and this can be used to advantage to reduce the computation time.

Since the data analysis is performed after a flight and all the flight data are available, the estimation accuracy can be improved by further processing call "smoothing". Using the intermediate results of the EKF, and by introducing adjointed variables, the MBFS achieves smoothed estimates of the states.[20] The algorithm of the smoother is given by:

**End Condition** The adjoint variables $\underline{\lambda}$ and $\Lambda$ are initialized according to eq. (17) and eq. (18).

$$\underline{\lambda}(T-) = -H_N^T D_N^{-1} \Delta \underline{z}_N \tag{17}$$

$$\Lambda(T-) = H_N^T D_N^{-1} H_N \tag{18}$$

where

$$D_N = H_N(-) P_N(-) H_N^T(-) + R_N \tag{19}$$

$$\Delta \underline{z}_N = \underline{z}_N - \underline{h}(\underline{x}_N(-)) \tag{20}$$

**Propagation of Adjoint Variables** The numerical integration from $t_{k+1}(-)$ to $t_k(+)$ is performed on the eq. (21) and eq. (22).

$$\dot{\underline{\lambda}} = -F^T \underline{\lambda} \tag{21}$$

$$\dot{\Lambda} = -F^T \Lambda - (F^T \Lambda)^T \tag{22}$$

**Adjoint Variable Update** The updates of the adjoint variables at $t = t_k$ are obtained from eq. (23) and eq. (24).

$$\underline{\lambda}_k(-) = \underline{\lambda}_k(+) - H_k^T D_k^{-1} (\Delta \underline{z}_k + D_k K_k^T \underline{\lambda}_k(+)) \tag{23}$$

$$\Lambda_k(-) = (I - K_k H_k)^T \Lambda_k(+) (I - K_k H_k) + (H_k^T D_k^{-1} H_k) \tag{24}$$

**Smoothed Estimates**—The smoothed estimates of the state, $\underline{x}$, and the covariance, P, are computed as follows:

$$[\underline{x}_k(+)]_{Smooth} = [\underline{x}_k(+)]_{Filter} - P_k(+) \underline{\lambda}_k(+) \tag{25}$$

$$[P_k(+)]_{Smooth} = [P_k(+)]_{Filter} - P_k(+) \Delta_k(+) P_k(+) \tag{26}$$

Extensive temporary disk storage has been used to retain quantities that are generated during the filter computations. They are listed as follows:

$$\Delta \underline{z}_k,\ P_k(+),\ D_k^{-1},\ K_k,\ H_k(-),\ \text{and}\ D_k \tag{27}$$

**Model Structure Determination** The estimated aircraft state vector, $\underline{x}$, and the aerodynamic forces, $\underline{B}$, can be recast into an algebraic equation,

$$\underline{y} = X \underline{\theta} \tag{28}$$

where the matrix X is generated from the state vector, $\underline{x}$, and the column vector $\underline{y}$ is any one of the 6 aerodynamic components of the time sequence $\underline{B}(t_k)$. The unknown parameter vector $\underline{\theta}$ is determined using a stepwise-linear regression method.[21] The least square estimate of the parameter vector of equation (28) is given by,

$$\underline{\theta} = [X^T X]^{-1} X^T \underline{y} \tag{29}$$

The variance of the parameter estimate in its simplest form is given by,

$$\text{Var}(\underline{\theta}) = [X^T X]^{-1} (\sigma^2) \tag{30}$$

where $\sigma^2$ is the variance of the smoothed estimate $\underline{y}$. The data set contributing to the matrix X can be classified into several "subspacess", and the samples need not be drawn from a continuous flight test maneuver. The parameter vector $\underline{\theta}$ then is determined for each subspace, and a global model for the complete flight domain is obtained. The subspace classificatio is made on the basis of the angle of attack and the sideslip angle; hence, the stall characteristics can be determined with precision.

**Fisher Information Matrix**—From equation (30), the variance of the parameter vector is proportional to the matrix,

$$C = M^{-1} \tag{31}$$

where

$$M = X^T X \tag{32}$$

M is the Fisher Information Matrix normalized with respect to the variance, $\sigma^2$. When N samples are used to define X, an average Fisher Information Matrix can be defined as:

$$M_{Av} = (1/N) M \tag{33}$$

$M_{Av}$ should be nonsingular for the parameter estimator of equation (29) to be consistent.

**Parameter Uncertainty Estimate** Sufficient flight test data in each subspace are necessary for complete regression analysis using eq. (29), and the distribution of the data has a direct bearing on the confidence levels of the estimates as quantified by the $M_{Av}$.[11] Actual flight test results for an F-4S aircraft show reduced confidence in the parameters wherever the data distribution is sparse in any

particular ($\alpha$, $\beta$) region.[22] The Micro-MAP is programmed to assist the pilot using the "zero reader", where the ($\alpha$, $\beta$) measurements are displayed in real-time. The pilot tracks the cross needle of the "zero reader" by manipulating the cockpit controls.

**Control Inputs** The estimation accuracy of the parameter vector can be improved by suitably designing the control inputs. Certain elements of the matrix M are crucial to the performance of the parameter estimation algorithm.[23] The Micro-MAP is, therefore, programmed to compute five elements of $M_{AV}$ for each maneuver. The five elements are $\underline{\delta E}^T\underline{\delta A}$, $\underline{\delta E}^T\underline{\delta R}$, $\underline{\delta A}^T\underline{\delta R}$, $\underline{\delta E}^T\underline{\alpha}$, and $\underline{\alpha}^T\underline{\beta}$. In the Avionics Research Aircraft identification, the $\underline{\alpha}^T\underline{\beta}$ element particularly gave trouble as a result of high correlation.[3] Following each maneuver, the pilot makes a decision whether to perform a new maneuver or to repeat the previous maneuver depending on the cross-correlation of the variables.

**Flight Test Results** For the initial flight tests, the maneuvers were designed to have low accelerations. Each maneuver lasted for 25-35 sec, starting with a 5-sec trim and ending with another 5-sec trim. Initial trim flight is necessary to estimate the attitude and the initial condition of the sailplane; sensor biases also can be computed. The flight test data obtained from one maneuver corresponding to a mixed input are presented in **Figure 15**. The data will be used for the estimation of parameters using the algorithms so far described. The locus of the control stick was a square. The rudder was in phase with the elevator deflection. These inputs were unconventional, and the resulting motion was disorienting to the pilot. The different velocity and angle of attack time histories measured on each wing tip show the positional dependence of the data. The wing tip boom vibration on the air data measurements is not significant. The altitude dropped at a rate of 300 ft. per min. With an initial altitude of 5000 ft, and 3100 ft reserve, flight testing can be conducted for about 10 min.

## CONCLUSION

An instrumentation package suitable for high angle of attack and sideslip flight condition has been designed and flight tested. The data acquisition system is a microprocessor-based system. High data quality is achieved by analog filtering before sampling. Simple statistical and display techniques are used to monitor the subsystem failure. Portability of the Micro-MAP is achieved by modularizing the hardware. The bootstrap procedure allows the Micro-MAP to be an independent flight test instrument. By displaying the angle of attack and sideslip angle information to the pilot, the data base required for parameter identification can be acquired systematically. The control and state correlations that may degrade the performance of the regression algorithms are computed in flight. The algorithms required for identification and a time history of a coupled maneuver that will be used by the algorithms have been presented.


## ACKNOWLEDGEMENT

The Micro-MAP system has been developed and flight tested with support from The Schultz Foundation of Clifton, New Jersey. The Schweizer 2-32 sailplane has been lent to the Flight Research Laboratory by the National Soaring Museum, Elmira, New York. W.B. Nixon performed the flight tests. G.E. Miller provided flight test engineering support, and C. Fratter implemented the parameter identification algorithms.


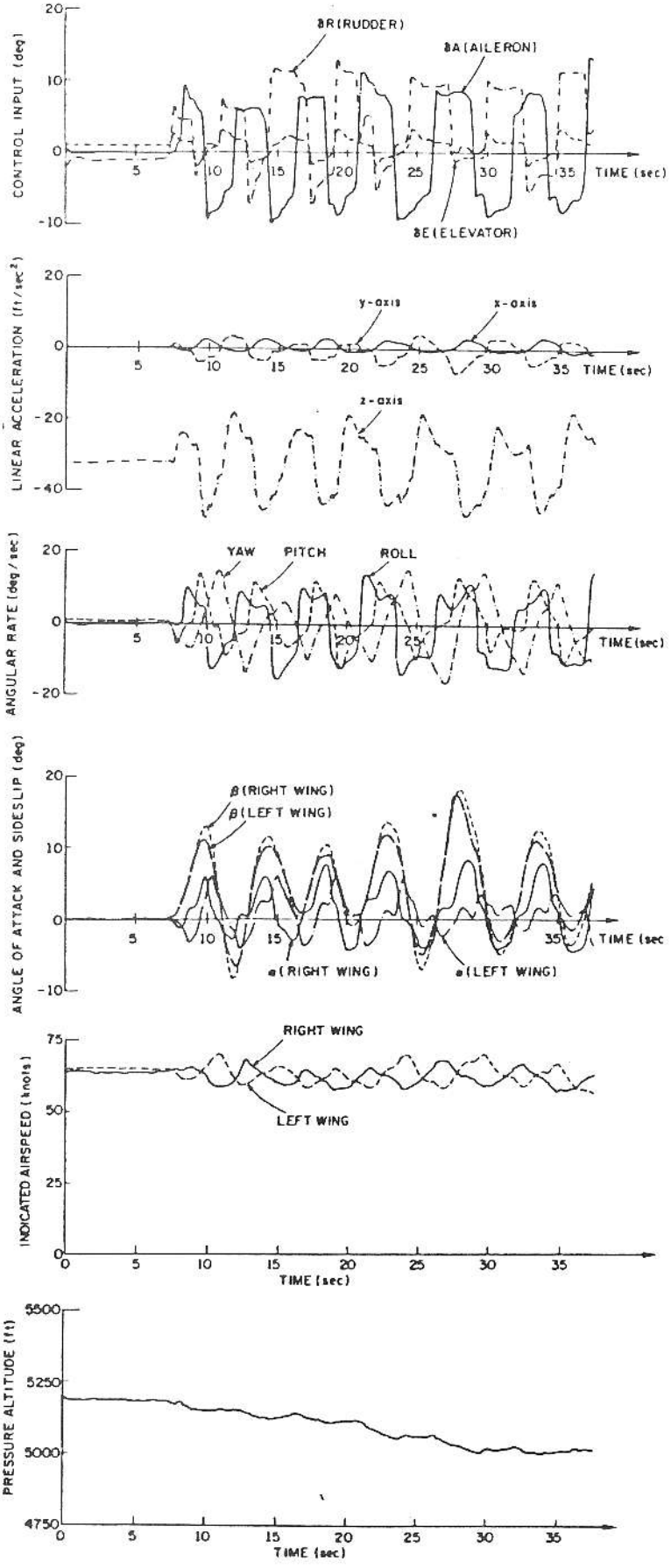


Figure 15: Initial Flight Test Results of a Coupled Maneuver

## NOMENCLATURE

$\underline{B}$ Aerodynamic force/moment
C Cramer-Rao bound
D Predicted covariance matrix (measurement)
F Gradient matrix (dynamics)
$\underline{f}$ Nonlinear function (dynamics)
H Gradient matrix (measurements)
H(s) Filter transfer function
$\underline{h}$ Nonlinear function (measurement)
I Identity matrix
K Kalman gain matrix
k Sampling instant index
L Matrix for Gauss-Markov process
M Fisher information matrix
N Number of samples or last sample of the data
P State covariance matrix
$p_d$ Dynamic pressure, psf
$p_s$ Static pressure, psf
Q Process noise covariance matrix
R Measurement noise covariance matrix
s Laplace operator
T Time of the last sample
t Time, sec
$\underline{v}$ Gaussian measurement noise
$\underline{w}$ Gaussian "process noise"
X Experimental matrix
$\underline{x}$ Aircraft state vector
$\underline{y}$ Regression variable vector
$\underline{z}$ Measurement vector

$\alpha$ Angle of attack, rad
$\beta$ Sideslip angle, rad
$\delta A$, $\delta E$, $\delta R$ Aileron, Elevator, and Rudder deflections
$\underline{\theta}$ Parameter vector
$\sigma$ Standard deviation
$\underline{\lambda}$ Adjoint vector for smoother or flow angle, radians
$\Lambda$ Adjoint matrix
$\Delta \underline{z}_k$ Predicted residual vector of measure at $t=t_k$
$(\ )^{-1}$ Matrix inverse
$(\ )^T$ Matrix transpose
$(\dot{\ })$ Dervative with respect to time
$\partial(.)/\partial x$ Partial derivative with respect to x

ADC Analog-to-digital converter
ADU Air data unit
ARA Avionics Research aircraft
CDU Control display unit
CPU Central processing unit
DAC Digital-to-analog converter
EBM Estimation-Before-Modeling
EKF Extended Kalman filter
IMU Inertial measurement unit
I/O Input and/or output
LED Light emitting diode
MBFS Modified Bryson-Frazier Smoother
Micro-MAP Microprocessor based system for the Measurement of Aerodynamic Parameters
PROM Programmable read-only memory
RAM Random access memory

## REFERENCES


1. Taylor, L.W., Iliff, K.W., and Powers, B.G., "A Comparison of Newton-Raphson and Other Methods for Determining Stability Derivatives from Flight Data", AIAA Paper No. 69-315, 1969.
2. Stalford, H.L., and Ramachandran, S., "Application of Estimation-Before-Modeling (EBM) System Identification Method to the High Angle of Attack/Sideslip Flight of T-2C Jet Trainer Aircraft – Vol II, Simulation Study Using T-2C Wind Tunnel Model Data", Report No. NADC-76097, June 1978.
3. Fratter, C., "Determination of Aerodynamic Coefficients for the Avionics Research Aircraft Using the Estimation-Before-Modeling Technique", M.S.E. Thesis, 1591-T, Department of Mechanical and Aerospace Engineering, Princeton University, Oct. 1982.
4. Sri-Jayantha, M., and Stengel, R.F., "A Microprocessor-based Data Acquisition System for Stall/Spin Research", to appear in IEEE Transactions on Aerospace Electronic Systems, (also AIAA Paper No. 81-2177).
5. Rediess, H.A., "An Overview of Parameter Estimation Techniques and Applications in Aircraft Flight Testing", NASA TN D-7947, Apr. 1973, pp. 1–18.
6. Iliff, K.W., and Maine, R.E., "NASA Dryden's Experience in Parameter Estimation and Its Uses In Flight Test", AIAA 9th Atmospheric Flight Mechanics Conference, AIAA-82-1373, Aug.1982.
7. Howard, J., "The Determination of Lateral Stability and Control Derivatives from Flight Data", Canadian Aeronautics and Space Journal, Mar. 1967, pp. 127–134.
8. Fredreich, H., "Determination of Stability Derivatives from Flight Test Results by Means of the Regression Analysis", AGARD-CP-172, May 1975, pp. 20-1 to 20-8.
9. Wingrove, R.C., "Estimation of Longitudinal Aerodynamic Coefficients and Comparison with Wind-Tunnel Data", NASA TN D-7947, Apr. 1974, pp. 125-147.
10. Gerlach, O.H., "The Determination of Stability Derivatives and Performance Characteristics from Dynamic Maneuvers", AGARD-CP-85, May 1971, pp. 16-1 to 16-23.
11. Klein, V., "Identification Evaluation Methods", AGARD-LS-104, Nov. 1979, pp. 2-1 to 2-21.
12. Gracey, W., "Measurement of Aircraft Speed and Altitude", NASA RP 1046, May 1980.
13. Schnieder, J.S., "The Effect of Placing Static Ports on a Kiel-Pitot Tube Behind the Kiel Tube Outlet Ports", Undergraduate Independent Work, Department of Mechanical and Aerospace Engineering, Princeton University, May 1982.
14. Gardenhire, L.W., "Sampling and Filtering", AGARD-AG-160, Vol. 1, 1976, pp. 6-1 to 6-12.
15. Katz, P., "Digital Control Using Microprocessors", Prentice Hall, Inc., Englewood Cliff, 1981.
16. Hamel, A., "Determination of Aircraft Dynamic Stability and Control Parameters from Flight Testing", AGARD-LS-114, May 1981, pp. 10-1 to 10-21.
17. Gelb, A., "Applied Optimal Estimation", MIT Press, Cambridge, Sept. 1980.
18. Carlson, N.A., "Fast Triangular Formulation of the Square Root Filter", AIAA Journal, Vol II, No. 9, Sept. 1973, pp. 1259-1265.
19. Tapley, B.D., and Peters, J.G., "Sequential Estimation Algorithm Using a Continuous $UDU^T$ Covariance Factorization", Journal of Guidance and Control, Vol. 3, No. 4, July-Aug. 1980, pp. 326-331.
20. Bierman, G.J., "Fixed Internal Smoothing with Discrete Measurements", International Journal of Control, Vol. 18, No. 1, 1973, pp. 65-75.
21. Klein, V., "Determination of Airplance Model Structure from Flight Data by Using Modified Stepwise Regression", NASA-TP-1916, 1981.
22. Trankle, T.L., Vincent, J.H. and Franklin, S.N., "System Identification of Nonlinear Aerodynamic Models", AGARD-AG-256, Mar. 1982, pp. 7-1 to 7-26.
23. Wells, W.R., and Ramachandran, S., "Multiple Control Input Design for Identification of Light Aircraft", IEEE Transaction on Automatic Control, Vol. AC-22, No. 6., Dec. 1977, pp. 985–987.